Precursor effects and successive phase transitions in a dilute crystal of KTN

1997 J. Phys.: Condens. Matter 9 10249

(http://iopscience.iop.org/0953-8984/9/46/022)

J. Phys.: Condens. Matter **9** (1997) 10249–10260. Printed in the UK PII: S0953-8984(97)85892-4

Precursor effects and successive phase transitions in a dilute crystal of KTN

Elghalia Bouziane† and Marc D Fontana‡

Laboratoire Matériaux Optiques à Propriétés Spécifiques, CLOES, University of Metz and Supelec, 2 Rue E Belin, 57078 Metz Cédex 3, France

Received 11 July 1997

Abstract. The light depolarization and Raman scattering spectrum have been measured as a function of the temperature in a dilute crystal of potassium tantalate niobate (KTN) with 2% Nb. The careful analysis of the Raman data versus temperature clearly reveals for the first time the sequence of two phase transitions below the cubic phase around 40 K and 32 K, connected to the dipolar ordering. The occurrence, well above 40 K, of Raman lines unexpected from the symmetry and attributed to the phonon density of states, as well as the quasi-elastic scattering, is interpreted in terms of the precursor phenomena and dynamic clusters in the cubic paraelectric phase.

1. Introduction

Solid solutions of potassium tantalate niobate $KTa_{1-x}Nb_xO_3$ (KTN) are of great interest regarding the microscopic origin of phase transitions. Replacing tantalum by niobium ions in the highly polarizable material $KTaO_3$ induces a change of the properties which can be adjusted between those of $KTaO_3$ and $KNbO_3$. While pure $KTaO_3$ is an incipient ferroelectric which does not undergo any phase transition, replacing Ta by Nb destabilizes the lattice and leads to a transition temperature which is strongly dependent on the Nb content.

The phase diagram of KTN ($0 \leqslant x \leqslant 1$) obtained from various experimental techniques [1] shows that at low Nb concentrations ($0.008 \leqslant x < x_c$), KTN presents a single and direct transition from the cubic phase to the rhombohedral phase, but a sequence of phase transitions as for pure $KNbO_3$ for concentrations $x \geqslant x_c$. The value of the critical concentration x_c for the occurrence of successive phase transitions is still debated. The value $x_c = 0.05$ [1] was accepted for a long time but a lower value $x_c = 0.03$ [2] was recently suggested.

A particular feature of the KTN system is the presence of unexpected Raman lines in the paraelectric (PE) phase. These new lines were attributed to first-order Raman scattering at the zone centre normally forbidden by cubic symmetry [3, 4]. In spite of intensive investigations carried out on KTN crystals, the number, nature and mechanism of the phase transitions, as well as the origin of the lines detected above T_c remain the object of current controversies, specially for low Nb concentrations [4–8].

† Permanent address: Laboratoire de Physique des Matériaux, Faculté des Sciences Aîn Chock, Université Hassan II, Casablanca, Morocco.

‡ Corresponding author. E-mail address: fontana@ese-metz.fr

0953-8984/97/4610249+12$19.50

Raman studies on KTN with $x = 1.2$ and 4% [4, 9] were devoted to the high-frequency lines, the so-called hard modes. The results have shown the presence of polar micro-regions in the paraelectric phase revealed by the existence above T_c of a hard mode TO_2 at 200 cm^{-1}, which was attributed to the first-order Raman scattering. Further, the appearance of the TO_3 line lying at 277 cm^{-1}, just at T_c was used to define the temperature of the structural transition. These last investigations were not concerned with the low-frequency spectrum which generally yields information on the phase transition associated with the soft mode and the central peak, if they exist.

In our study we pay attention to Raman measurements over a large frequency range, so that we relate the features at low frequency to the possible change observed at higher frequency in the hard modes. The KTN crystal used in our study is a dilute crystal with 2% Nb which is close to the critical concentration x_c. Anomalies revealed by Raman scattering are compared with information derived from the light depolarization and the second-harmonic generation (SHG) measurements, on the same $KTa_{0.98}Nb_{0.02}O_3$ crystal. In this paper we are specially concerned with the following aims: (1) to give an insight into the number and mechanism of the transition(s) in a crystal with Nb concentration lower than x_c; (2) to study the link between the occurrence of a quasi-elastic scattering (QES) and additional lines in the cubic phase and the precursor ordering phenomenon; (3) to interpret the origin of the new lines detected at high temperature. We show that they correspond neither to usual first-order Raman nor the normal second-order processes but can be attributed to the phonon density of states.

The paper is presented as follows. First, the light transmission and second-harmonic generation (SHG) measurements are used to obtain some evidence of two temperature transitions. Then the Raman scattering spectra are reported as a function of the temperature and carefully analysed. We specially emphasize the characteristics (frequency, width and integrated intensity) of each Raman peak which are plotted versus temperature. All results are discussed in section 3 and finally summarized in section 4.

2. Experimental results

2.1. Light transmission measurements

We determine the possible phase transition temperatures by the study of any change in the depolarization of the light transmitted through the crystal. We have recorded the transmitted intensity between parallel ($I_\parallel$) and crossed polarizers ($I_\perp$). The depolarization ratio R as defined by

$$R = \frac{I_\parallel - I_\perp}{I_\perp + I_\parallel} \tag{1}$$

is plotted as a function of the temperature in figure 1 and compared with the second-harmonic generation intensity I (SHG), measured in the same crystal [10]. On cooling, the behaviour of R displays anomalies around $T_1 \cong 40$ K and $T_2 \cong 32$ K. Above T_1, the light is not depolarized so that the optical properties of the crystal are isotropic, which confirms the cubic and centrosymmetric structure of the high-temperature phase. Between T_1 and T_2, the transmitted light is depolarized so that the optical properties are anisotropic rendering the crystal birefringent. Below T_2, the optical anisotropy of the crystal is continuously enhanced on cooling, then remains constant below 20 K. This change of the transmitted light through the crystal is the signature of depolarization due to multiple alterations of the polarization by the various domains caused by the structural changes.

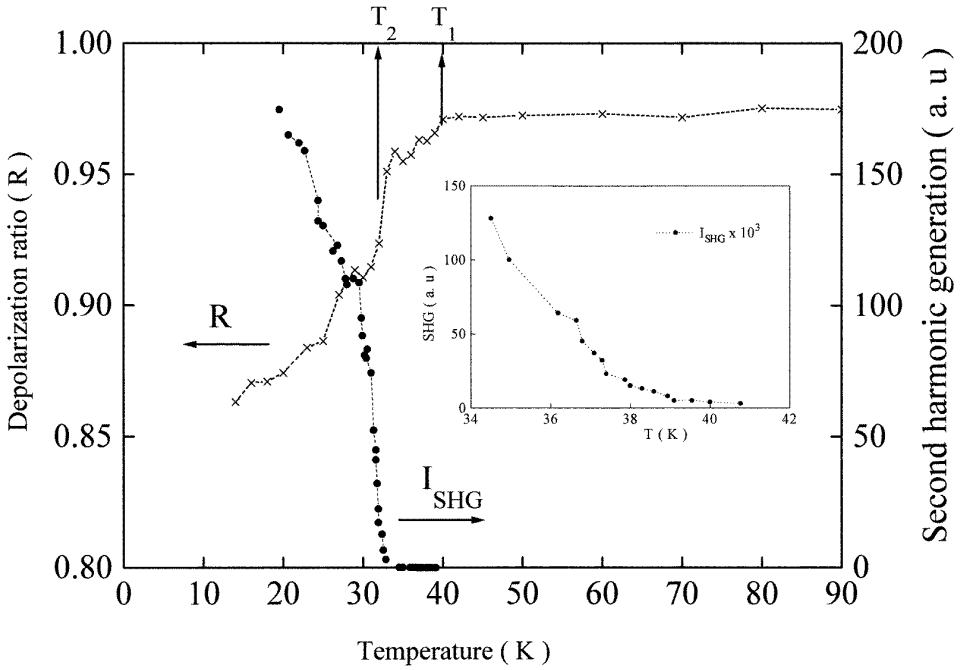

Figure 1. Temperature dependences of the depolarization ratio in the transmitted light and the second-harmonic generation (SHG) intensity [10] measured on $KTa_{0.98}Nb_{0.02}O_3$. The inset shows the value of I (SHG) above 32 K. Anomalies at the temperatures T_1 and T_2 are denoted by vertical arrows.

The temperatures T_1 and T_2, which are evidenced by the light transmission, are corroborated by anomalies observed in the SHG results [10]. These authors attributed a large increase of the SHG signal around 32 K to phase transition from the cubic phase to the rhombohedral structure and the remanent intensity (see inset of figure 1) above T_c to precursor effects. In our opinion, the presence of SHG between 40 K and 32 K arises from a first symmetry breaking since the SHG signal occurs only in a crystal without an inversion centre. From these results, we can hereafter define three temperature ranges: the high temperature range ($T > 40$ K), the intermediate temperature range ($32\ \text{K} < T \leqslant 40$ K) and the low temperature range ($T \leqslant 32$ K).

2.2. Raman measurements

Raman measurements were carried out in right-angle scattering geometries on a $KTa_{0.98}Nb_{0.02}O_3$ crystal with cut (100) faces. Spectra were obtained with a Spex double monochromator using the 632.8 nm He–Ne laser line. The incident and scattered light were generally directed along the z and x axes, respectively and the spectra were measured under the same experimental conditions. These conditions are only changed when the measurements are recorded at low frequencies instead of the data obtained in a complete frequency range.

2.2.1. Raman spectra as a function of the temperature. Figure 2 shows the spectrum recorded in two configurations at 100 K. This spectrum displays broad second-order

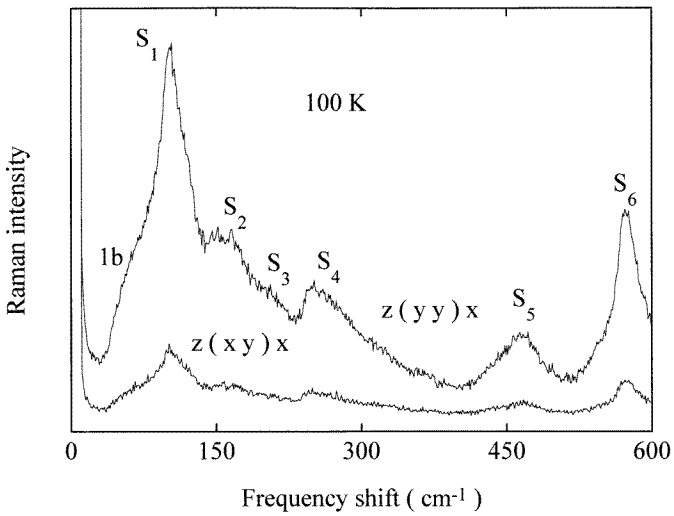

Figure 2. Polarized Raman spectra recorded in two configurations $z(yy)x$ and $z(xy)x$ at 100 K in $KTa_{0.98}Nb_{0.02}O_3$. x, y and z are the cubic axes.

scattering bands denoted S_1 to S_6, characteristic of the cubic structure. Thus the $z(yy)x$ scattering corresponds to the two phonon lines of the symmetries E_g and A_{1g} whereas the $z(xy)x$ scattering, as well as the equivalent to $z(xz)x$ and $z(yz)x$ scattering, gives rise to F_{2g} modes. The Raman spectrum obeys to the cubic selection rules for all temperatures down to 40 K. Below 40 K, the intensities of the spectra carried out in $z(xy)x$ and $z(yz)x$ scattering are different from each other and much smaller than the $z(yy)x$ spectrum. This is consistent with the occurrence of the phase transition at T_1.

Figures 3 and 4 exhibit the low- and high-frequency spectra recorded in the $z(yy)x$ scattering, for various temperatures within the same experimental conditions, between 0 and 120 cm^{-1} and 150 and 600 cm^{-1} respectively. The spectrum displays a significant but monotonic change as a function of the temperature at low and high frequency ranges.

In the low-frequency range (below 60 cm^{-1}) reported in figure 3 we can distinguish two features: a quasi-elastic scattering (QES) below 15 cm^{-1} as a tail of the Rayleigh line and a broad scattering above 15 cm^{-1}. Both features monotonically increase in intensity between 100 and 40 K. Two broad bands denoted as 1a and 1b emerge from this scattered intensity and become more and more resolved when the temperature decreases. Below 35 K, the QES and the peaks 1a and 1b have quite different behaviours since these lines continuously increase in intensity whereas the QES progressively vanishes.

As shown in figure 4, the spectrum in the high frequency range displays new lines (lines 2 and 4) which occur around 200 cm^{-1} and 545 cm^{-1} respectively for the temperatures below 60 K, and an additional peak, denoted 3, which is detected around 280 cm^{-1} below 38 K. All these lines are more and more intense and narrow with decreasing temperature. It can be pointed out that the lines 1, 2 and 4 exist above $T_1 \cong 40$ K whereas the line 3 appears only close to this transition temperature. Whereas the second-order bands decrease in intensity as expected when the temperature descreases, all new lines display a surprising increase in intensity. All appear as well resolved lines in the low-temperature phase ($T < T_2$) like usual first-order phonons. However, whereas each line 1b, 2, 3 and 4 is located around the same frequency on both sides of T_2, the line 1a exhibits a clear increase of the frequency when the temperature is lowered below $T_2 \cong 32$ K.

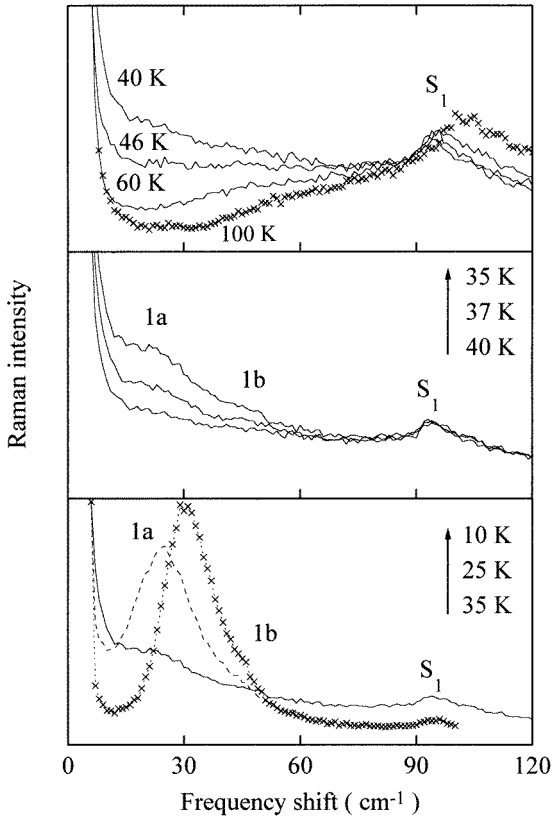

Figure 3. Low-frequency Raman spectra recorded at various temperatures in $KTa_{0.98}Nb_{0.02}O_3$.

2.2.2. Analysis of Raman results. In order to analyse more carefully the experimental data as a function of the temperature and to study their possible relation with the phase transitions, we determine successively the integrated intensity, frequency and damping of each line.

Integrated intensity. We report in figure 5 the temperature dependence of the integrated intensity of the quasi-elastic scattering and the new lines, as calculated from

$$J = \int_a^b \frac{I(\omega)}{\omega[n(\omega)+1]}\,\mathrm{d}\omega \tag{2}$$

where a and b correspond to the low- and high-frequency limits of the peak, $n(\omega)$ is the Bose–Einstein population factor and $I(\omega)$ denotes the experimental scattered intensity.

We note in the upper part (a) of figure 5 that the broad maxima of the intensity $J(\mathrm{QE})$ seemingly coincide with the temperatures $T_1 \cong 40$ K and $T_2 \cong 32$ K, as defined from the light depolarization and the SHG measurements. We can also remark that the temperature T_1 corresponds to the appearance of the line 3 whereas T_2 seems to be related to the main maximum of the intensities $J(\mathrm{QE})$, $J(1)$, $J(2)$ and $J(4)$. The integrated intensity of each line increases weakly between 60 K and $T_1 \cong 40$ K, then more strongly between T_1 and T_2 and finally, after an anomaly at T_2, continues to rise gently below T_2.

All these results show that the lines 1, 2 and 4 and the QES on one hand and the line 3 on the other hand have different origins. We note also that the temperature dependence of

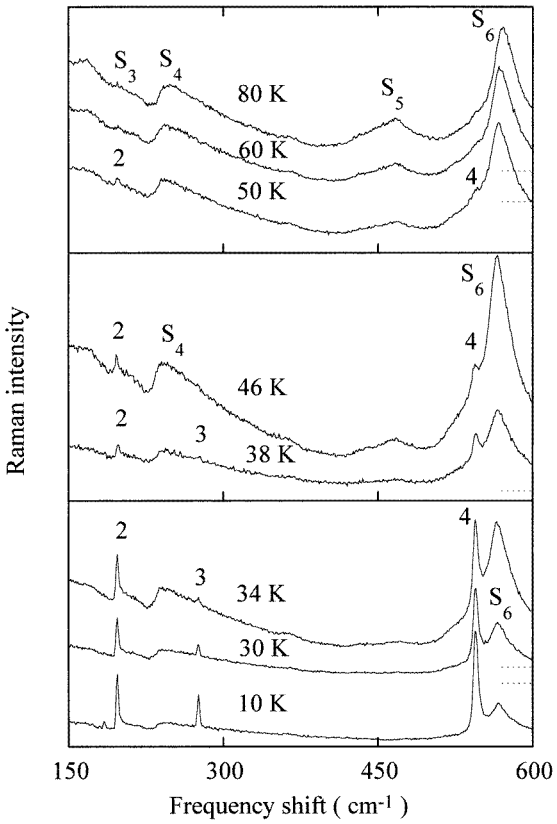

Figure 4. High-frequency Raman spectra recorded at various temperatures in $KTa_{0.98}Nb_{0.02}O_3$.

the intensity for new lines is very different to the behaviour of the second-order scattering intensity which decreases when the temperature decreases.

Frequency and damping. We have adjusted Raman spectra, recorded in the whole temperature range, to establish the behaviour of the peak parameters (linewidth and frequency), specially on both sides of the transition temperatures defined above. In these calculations, the second-order scattering contribution and the background were eliminated. The low-frequency Raman spectra were fitted to a sum of decoupled relaxator and damped harmonic oscillators of the type

$$I_R(\omega) = \frac{I(\omega)}{\omega[n(\omega)+1]} = \sum_{j=1}^{2} K_j \frac{\omega_j^2 \Gamma_j}{(\omega_j^2 - \omega^2)^2 + \omega^2 \Gamma_j^2} + K' \frac{\gamma_r}{\omega^2 + \gamma_r^2} \qquad (3)$$

where ω_j and Γ_j are the frequency and damping of the phonon j (lines 1a and 1b) respectively, γ_r is the inverse relaxation time, K_j and K' are the intensity factors for the oscillator j and the relaxator strength respectively.

The high-frequency modes (lines 2, 3 and 4) are fitted to damped harmonic oscillators. Some examples of the fit are reported in figure 6. A good agreement is achieved between the experimental data and the calculated values.

Our low-frequency Raman results are compared with the hyper-Raman (HR) data, as obtained in the cubic phase of the same crystal [10]. In principle, Raman and hyper-Raman

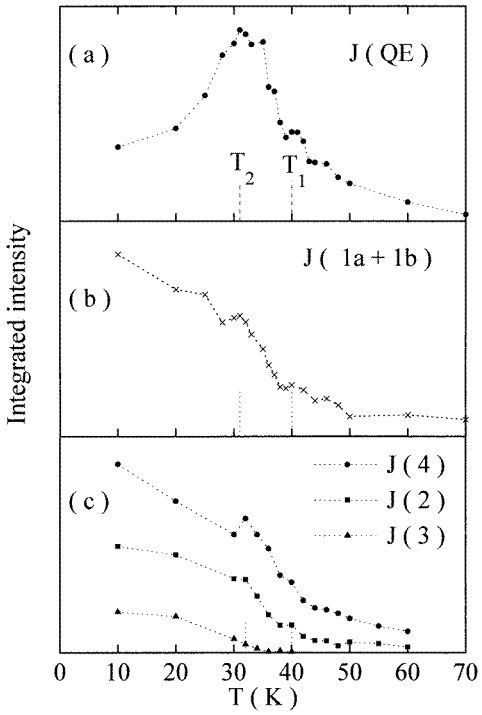

Figure 5. Temperature dependence of the integrated intensity for the quasi-elastic scattering $J(\mathrm{QE})$, the low-frequency peaks $J(1a + 1b)$ and the hard modes $J(2)$, $J(3)$ and $J(4)$ in $KTa_{0.98}Nb_{0.02}O_3$. The temperatures T_1 and T_2 are denoted by vertical dashed lines.

measurements do not provide the same information since only the infrared active one-phonon scattering can be detected in the case of HR experiments. It is therefore not very surprising to observe the large discrepancy between HR and Raman spectra recorded in the cubic phase of KTN with 2% Nb, as reported in figure 7. Nevertheless this result clearly shows that the broad Raman scattering cannot derive from the simple activation of the TO_1 phonon. To be more consistent with the Raman data which show a QES phenomenon (see figure 3), the treatment of the HR results is reconsidered, in using a fit of data to a coexisting central peak and damped oscillator. Results obtained in this new fitting procedure are shown in figure 7 and are used below among others to discuss the temperature dependence of the mode parameters.

The calculations show that the high-frequency modes labelled 2, 3 and 4 have a frequency independent of the temperature but their linewidth largely varies in the high- (for the line 4) and intermediate-temperature phases (for each line). Figure 8 shows that the linewidth of the peak 4 is much larger in the high-temperature cubic phase than in the low-temperature phase, and decreases strongly with decreasing temperature, presenting changes of slope at transition temperatures T_1 and T_2. The linewidth of the peak 2 shows a similar behaviour as for the peak 4, with an anomaly at T_1. In the low-temperature phase, each linewidth is nearly constant.

Frequencies and widths for low-frequency peaks are shown in figure 9. Below T_2, the frequency of the phonon 1a increases with falling temperature whereas the 1b phonon frequency is nearly constant. This means that the lowest-frequency mode of the cubic phase,

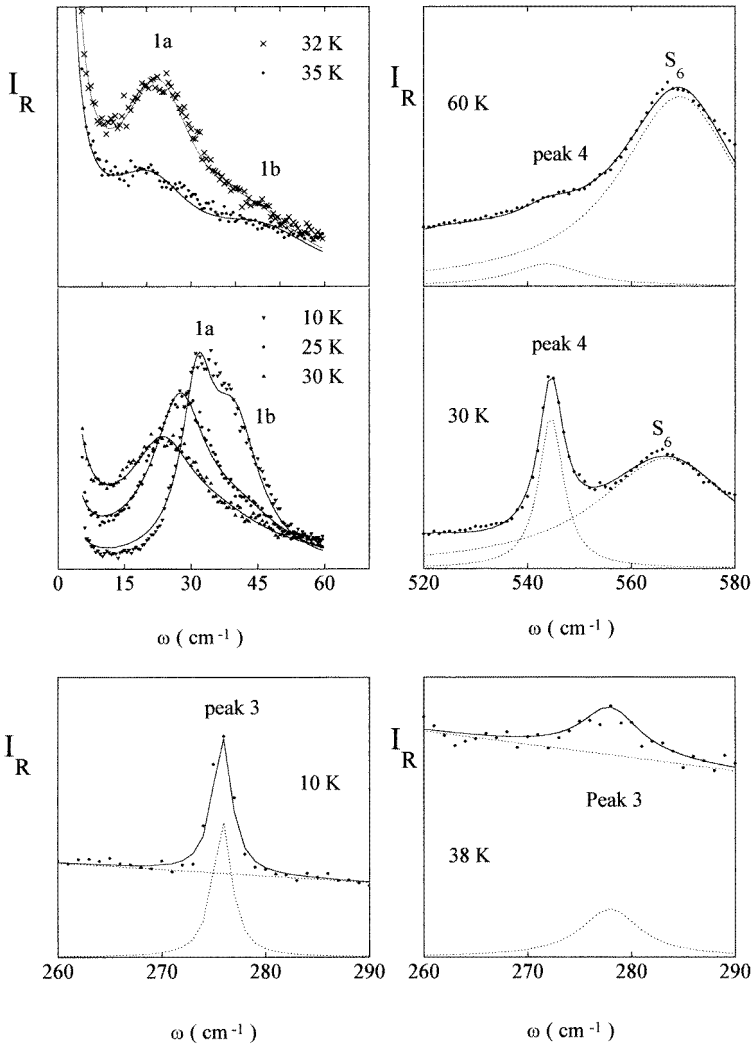

Figure 6. Typical Raman spectra fitted to damped harmonic oscillators or using (3) (see text). Experimental data are represented by symbols. The dashed curves are calculated spectra, corrected by the second-order scattering and the background.

which clearly softens with decreasing temperature, splits at T_1 into two modes which harden in the lowest-temperature phase.

In the cubic phase, above T_1, the widths of lines 1a and 1b are relatively large and independent of the temperature. Then they abruptly decrease on cooling below 40 K. Finally in the low-temperature phase, the damping is relatively small for both phonons, reflecting their stability. We can also note that above 40 K (T_1), the linewidths of the bands 1a and 1b, as deduced from fit to Raman data, are found much larger than the damping $\Gamma(\mathrm{TO}_1)$ as derived from HR results. Indeed we find the widths of 49 cm^{-1} and 45 cm^{-1} for lines 1a and 1b whereas the damping of TO_1 is 16 cm^{-1}. This analysis shows that these parameters are not really linked on both sides of the transition temperature. Consequently the lines

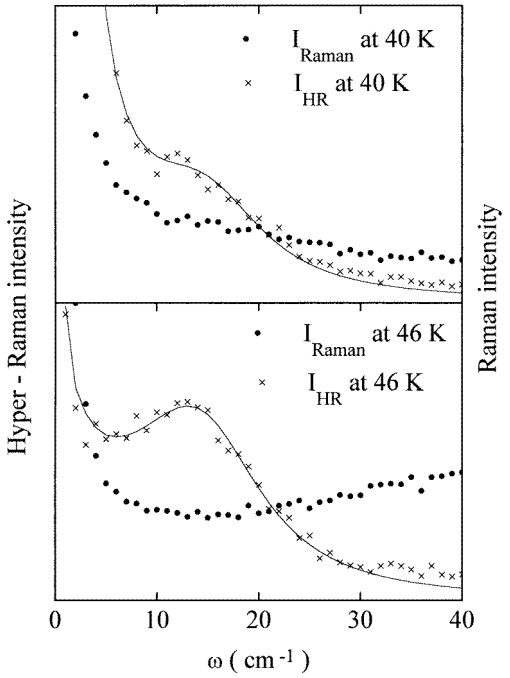

Figure 7. Comparison between hyper-Raman (HR) spectra and the Raman spectra recorded at the same temperatures in KTN with 2% Nb. Experimental data are represented by symbols. The continuous line is the hyper-Raman spectrum fitted to a model based on the coexistence of a central relaxational peak and a damped oscillator corresponding to the soft mode. Note the large broadening of the low-frequency tail in the HR spectrum between 46 and 40 K.

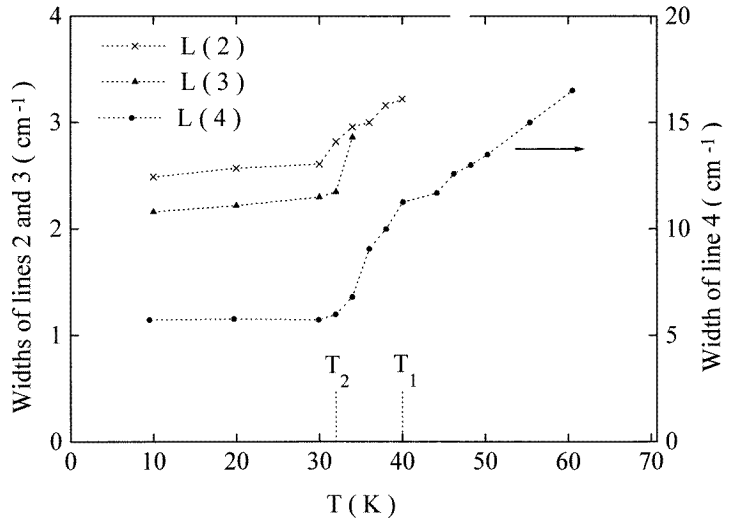

Figure 8. Temperature dependence of the widths for the lines 2 (×), 3 (▲) and 4 (●) in $KTa_{0.98}Nb_{0.02}O_3$.

detected at low frequency in Raman scattering and hyper-Raman scattering have clearly

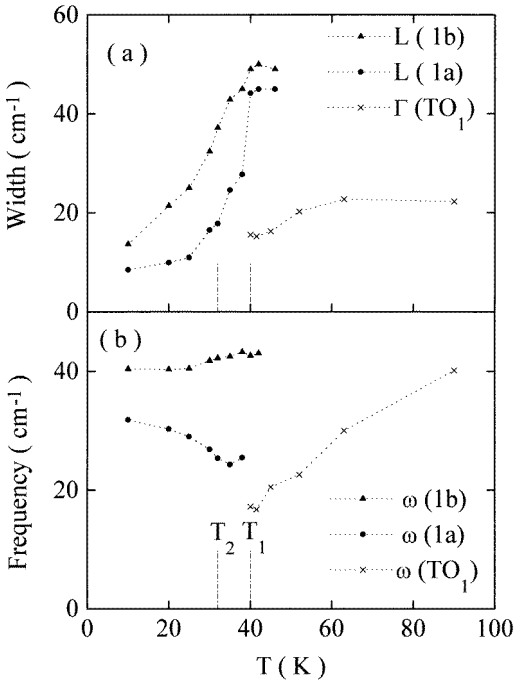

Figure 9. Temperature dependence of the widths (a) and frequencies (b) of the Raman peaks 1a (●) and 1b (▲) in $KTa_{0.98}Nb_{0.02}O_3$. The damping (a) and frequency (b) of the soft mode TO_1, detected by hyper-Raman measurements on the same crystal, are represented by the symbols (×).

different origins.

3. Discussion

Results obtained from the light depolarization, the SHG and the Raman scattering measurements clearly reveal anomalies around two temperatures $T_1 \cong 40$ K and $T_2 \cong$ K characterizing the phase transitions below the cubic phase in KTN with 2% Nb. These temperature transitions can be defined by maxima in the integrated intensity of the QES and the lines 1, 2 and 4 whereas T_1 is particularly related to the occurrence of the line 3.

At high temperature ($T > 40$ K), the lack of depolarization of the light, the absence of the SHG signal as well as the presence of the large second-order phonon scattering in the spectrum obeying selection rules, according to the centrosymmetric crystal, are consistent with the cubic structure of the phase.

We have noted that the line 3, which is related to the non-polar character of the transverse optical phonon (out of phase motion of two oxygen ions [11]), occurs close to T_1. Its appearance coincides, on one hand, with the peak in the plot of the integrated intensities $J(\mathrm{QE})$, $J(1)$, $J(2)$ and $J(4)$ and, on the other hand, with changes in the optical anisotropy as well as the detection of the SHG signal. The occurrence of this phonon is thus connected to a structural change [4, 9].

The QES can be explained by the relaxation of the off-centring Nb ions with a time scale of 10^{-8} s [12] between two equivalent positions. This process was invoked to interpret the large frequency dispersion of the dielectric behaviour in KTN crystals. This dispersion was

shown to be strongly dependent on both the crystal composition and the temperature [5]. The integrated intensity of the QES is related to the correlation length of the Nb fluctuations which are clearly linked to the mechanism of the phase transitions, as revealed by anomalies in the temperature dependence of the integrated intensity (see figure 5). Above T_1, these correlated off-centred Nb fluctuations constitute clusters in the cubic phase, which reveal a precursor and partial order of the low-temperature phases.

The presence of the unexpected lines 1, 2 and 4 in the cubic phase above T_1, and below 60 K, can be attributed to phonon density of states, activated by the off-centring of Nb ions. This origin was previously demonstrated in the KTN crystal with a larger (7%) niobium concentration [13]. This explanation is supported by the fact that the high-frequency modes are nearly independent of the temperature [14] and the wave vector [15].

All the additional peaks disappear at the structural phase transition temperature T_1 and give rise to normal first-order lines.

Now we turn to the origin and mechanism of the phase transitions.

The temperature T_1 is connected to both the appearance of the non-polar mode denoted 3 and the occurrence of the SHG intensity. Both features reveal that the first phase transition at T_1 is connected to a structural change leading to a non-centrosymmetric phase.

The correlation between relaxing dipoles associated with the motion of Nb ions increases, as revealed by the rapid increase of the integrated intensity $J(\mathrm{QE})$ and the dielectric permittivity [12], so that a second transition to a ferroelectric phase connected to the dipolar ordering takes place at $T_2 \cong 32$ K. The strong increase of the SHG intensity with decreasing temperature can be interpreted as an increase of the size of ordered regions from antiparallel to parallel polarization [16].

Since the distance between the two neighbouring Nb ions is relatively large, the size of clusters increases strongly on cooling and the long-distance polar ordering is not fully achieved. This explains the continuous increasing of each first-order Raman line intensity and the SHG signal. The ferroelectric clusters occupy just a fraction of the sample and thus have the possibility to occupy more and more of the space. This result is in conflict with the occurrence of one direct phase transition from the cubic phase to the rhombohedral phase. Our result is however in agreement with non-linear dielectric measurements [6], which show the occurrence of polarized clusters even for very low Nb contents ($0.0075 \leqslant x \leqslant 0.02$). Therefore the mechanism of phase transitions in KTN differs from what is usually expected in a ferroelectric material.

4. Summary

In this work we have carefully analysed the anomalies shown in a dilute KTN crystal (with 2% Nb) by the Raman scattering as well as the light depolarization and the SHG signal. We have for the first time pointed out the appearance of two successive phase transitions in this crystal at $T_1 \cong 40$ K and $T_2 \cong 32$ K respectively. We have also evidenced the presence of unexpected lines in the cubic phase between 60 K and T_1. These lines were attributed to the phonon density of states and reflect the occurrence of precursor order processes, as previously revealed by other techniques such as RMN [17] and EXAFS [18].

References

[1] Rytz D, Höchli U T and Bilz H 1980 *Phys. Rev.* B **22** 359
[2] Sommer D, Friese D, Kleemann W and Rytz D 1991 *Ferroelectrics* **124** 231
[3] Uwe H, Lyons K B, Carter H L and Fleury P A 1986 *Phys. Rev.* B **33** 6436

[4] Di Antonio P, Vugmeister B E and Toulouse J 1993 *Phys. Rev.* B **47** 5629
[5] Fontana M D, Maglione M and Höchli U T 1993 *J. Phys.: Condens. Matter* **5** 1895
[6] Bidault O and Maglione M 1997 *J. Physique* I **7** 543
[7] Gehring P M, Chou H, Shapiro S M, Hriljac J A, Chen D H, Toulouse J, Rytz D and Boatner L A 1992 *Phys. Rev.* B **46** 5116
[8] Sommer D, Kleemann W and Rytz D 1990 *Ferroelectrics* **106** 137
[9] Toulouse J, Di Antonio P, Vugmeister B E, Wang X M and Knauss L A 1992 *Phys. Rev. Lett.* **68** 232
[10] Kugel G E, Vogt H, Kress W and Rytz D 1984 *Phys. Rev.* B **30** 985
[11] Fontana M D, Metrat G, Servoin J L and Gervais F 1984 *J. Phys. C: Solid State Phys.* **16** 483
[12] Maglione M, Rod S and Höchli U T 1987 *Europhys. Lett.* **4** 631
[13] Bouziane E, Fontana M D and Kleemann W 1994 *J. Phys.: Condens. Matter* **6** 1965
[14] Rytz D, Fontana M D, Servoin J L and Gervais F 1983 *Phys. Rev.* B **28** 6041
[15] Foussadier L, Fontana M D and Kress W 1996 *J. Phys.: Condens. Matter* **8** 1135
[16] Voigt P and Kapphan S 1991 *Ferroelectrics* **124** 243
[17] Rod S, Borsa F and Van der Klink J J 1988 *Phys. Rev.* B **38** 2267
[18] Lyons K B, Fleury P A and Rytz D 1986 *Phys. Rev. Lett.* **57** 2207